Journal of Luminescence 170 (2016) 1–7

Contents lists available at ScienceDirect

Journal of Luminescence

journal homepage: www.elsevier.com/locate/jlumin

Up- and down-conversion emissions from Er^{3+} doped K_2YF_5 and K_2YbF_5 crystals

P.A. Loiko [a,*], N.M. Khaidukov [b], J. Méndez-Ramos [c], E.V. Vilejshikova [a], N.A. Skoptsov [a], K.V. Yumashev [a]

[a] Center for Optical Materials and Technologies (COMT), Belarusian National Technical University, 65/17 Nezavisimosti Avenue, Minsk 220013, Belarus
[b] N.S. Kurnakov Institute of General and Inorganic Chemistry, 31 Leninskii Prospekt, Moscow 119991, Russia
[c] Departamento de Física, Universidad de La Laguna, 38206 La Laguna, Tenerife, Spain

ARTICLE INFO

Article history:
Received 1 July 2015
Received in revised form
11 September 2015
Accepted 7 October 2015

Keywords:
Fluoride crystals
Erbium
Up-conversion
Down-conversion
Luminescence

ABSTRACT

Crystals of Er^{3+} doped K_2YF_5 and K_2YbF_5 as well as stoichiometric K_2ErF_5 have been grown under hydrothermal conditions. Peculiarities of Er^{3+} luminescence in these crystals have been studied under different excitation wavelengths and, in particular, it has been discovered that in 5 at% Er^{3+}:K_2YbF_5, the energy transfer (ET) efficiency from Yb^{3+} to Er^{3+} reaches 67%. Under near-IR excitation at 980 nm, this crystal is characterized by intense yellow up-conversion luminescence with CIE coordinates: $x=0.449$, $y=0.465$. Under UV and visible excitation at 355 and 532 nm, respectively, clear evidences of the down-conversion process through the cross-relaxation have been found. The corresponding efficiency of ET from Er^{3+} to Yb^{3+} is 69%. These features make Er^{3+}:K_2YbF_5 crystals attractive for developing luminescent up- and down-converters for enhancing the performance of solar cells.

1. Introduction

Up-conversion is a process when absorption of two or more low-energy pump photons is followed by an emission of one photon with a higher energy. Materials containing trivalent rare-earth ions like erbium (Er^{3+}) provide efficient up-conversion [1]. Er^{3+} ions can absorb light at around 980 nm which corresponds to the emission of well-developed InGaAs laser diodes and emit in both the green (~540 nm) and the red (~650 nm) spectral regions. Due to the special structure of Er^{3+} energy levels, several efficient processes that provide the population of the higher-lying excited states can be easily implemented namely excited-state absorption (ESA), cross-relaxation (CR) and energy-transfer (ET) [2]. The use of an Er^{3+}–Yb^{3+} couple is beneficial for increasing the up-conversion efficiency due to a rather strong absorption of the Yb^{3+} ions at ~1 μm. The potential applications of Er-doped phosphors are in the field of solid-state lighting [3], biological labeling [4,5] or enhancement of the solar-cell efficiency [6] as well as the data concerning Er^{3+} up-conversion visible lasers have been reported [7].

Down-conversion (that is frequently called quantum cutting) is a process when one high-energy photon (UV/visible) is cut into two lower energy photons (near-IR) [8]. This process can be very efficient for Yb^{3+}–RE^{3+} ions pairs (where RE stands for Tb, Pr, Tm, Er, Nd or Ho ions) [9,10]. Typically, absorption of UV/visible light by RE^{3+} ions leads to the emission of Yb^{3+} ions at ~1 μm corresponding to the $^2F_{5/2}\rightarrow{}^2F_{7/2}$ transition. Down-conversion is useful when considering the problem of spectral mismatch between the solar cells and solar spectrum. In particular, for the Er^{3+}–Yb^{3+} couple, absorption of sunlight by Er^{3+} in the UV/visible can lead to the Yb^{3+} emission with the energy matching the band gap energy of silicon [11]. The efficiency of such second-order down-conversion process depends strongly on the interionic distances between optically active ions and, thus, the materials with high rare earth ion concentrations are desirable. It is also important to note that down-conversion is a linear process [12] and thus it can be efficient even for non-concentrated sunlight.

An important point for the efficient up- and down-conversion is the vibronic properties of the host. The rate of non-radiative relaxation from the excited-states of RE^{3+} ions is lower for materials with a lower maximum phonon frequency ν_{max}. Thus, for such materials the lifetimes of RE^{3+} ions in the involved excited-states are longer which increases the probability of further excitation steps like ESA or CR leading in general to the increase of intensity of up- and down-conversion luminescence. For fluoride crystals, ν_{max}~400 to 600 cm^{-1} which is much lower as compared with their oxide counterparts (ν_{max}~1000 cm^{-1}). Indeed,

* Corresponding author.
E-mail address: kinetic@tut.by (P.A. Loiko).

http://dx.doi.org/10.1016/j.jlumin.2015.10.016
0022-2313/

Er^{3+} and Er^{3+}/Yb^{3+} doped fluoride and oxyfluoride materials (in the form of single crystals, glass–ceramics or nanopowders) provide intense up- and down-conversion luminescence [1–8].

In the present work, an attention is paid to the study of up- and down-conversion in fluoride K_2YF_5 crystals doped with Er^{3+} and Yb^{3+} ions as well as crystals of the stoichiometric compositions like K_2ErF_5 and K_2YbF_5 have been studied. Potassium yttrium pentafluoride, K_2YF_5, belongs to the orthorhombic system, space group $Pna2_1$ (33) [13]. In the K_2YF_5 structure each Y^{3+} ion is surrounded by seven F^- ions with C_{2v} symmetry and the YF_7 polyhedra form chains parallel to the *c*-axis. The intrachain Y^{3+}–Y^{3+} distance is around 3.7 Å, and the shortest distance between the ions of different chains reaches ~5 Å [14]. Such a structure is favorable for high doping concentrations of rare-earth ions. Indeed, isostructural series $K_2Y_{1-x}Er_xF_5$, $K_2Y_{1-x}Yb_xF_5$ and $K_2Y_{1-x-y}Yb_xEr_yF_5$ (with $0<x<1$ and $0<y<1$) exist. In addition, K_2YF_5 is characterized with a relatively low maximum phonon frequency $\nu_{max}\sim 418\ cm^{-1}$ [15] that is lower than in typical fluoride hosts, CaF_2 (477 cm^{-1}) or $LiYF_4$ (~490 cm^{-1}) and only slightly higher than in LaF_3 (~400 cm^{-1}). These features determine a potential for achievement of high up- and down-conversion efficiencies with rare-earth ion doped K_2YF_5. To the date, the spectroscopic properties of Nd^{3+} [16–19], Tb^{3+} [20], Pr^{3+} [21–24] and Tm^{3+} [25,26] ions in the K_2YF_5 have been studied. As for Er^{3+} ions, some data of crystal filed splitting and lifetime studies are reported for a K_2ErF_5 crystal in [27]. In [15], the up-conversion luminescence of Er^{3+} impurity ions in a Tm^{3+}:K_2YF_5 crystal has been studied and recently some data on the up-conversion luminescence in K_2YF_5 doubly doped with Er^{3+} and Yb^{3+} have been reported [28]. Relatively scarce information about this crystal is related to the difficulty of its synthesis.

2. Experimental

Crystals of orthorhombic K_2YF_5 and K_2YbF_5 doped with Er^{3+} as well as K_2ErF_5 and K_2YbF_5 were grown under hydrothermal conditions. For hydrothermal experiments, copper insert lined autoclaves having a volume of about 40 cm^3 were utilized and the inserts were separated into synthesis and crystallization zones by perforated diaphragms. The fluoride crystals were synthesized by a direct temperature-gradient method as a result of the reaction of the aqueous solutions containing 40–50 mol% KF with oxide mixtures $(1-x-y)Y_2O_3$–xEr_2O_3–yYb_2O_3 at a temperature of about 750 K in the synthesis zone, a temperature gradient along the reactor body of up to 3 K/cm, and a pressure of about 100 MPa. The purity of the utilized oxides was more than 99.99%. Under these conditions, spontaneously nucleated crystals up to 0.5 cm^3 in size were grown in the upper crystallization zone of the autoclave for 200 h.

The structure type and phase purity of synthesized samples were characterized with conventional powder X-ray diffraction (XRD) technique and powder XRD patterns were obtained by using a Bruker D8 Advance X-Ray powder diffractometer with Cu Kα radiation.

Absorption spectrum was measured for a 10 at% Er^{3+}:K_2YF_5 crystal with a Varian CARY 5000 spectrophotometer (the spectral bandwidth, SBW, was 0.1 nm).

Up-conversion luminescence (UCL) was excited by continuous-wave radiation of InGaAs laser diodes emitting at ~960 nm (excitation to the Er^{3+} $^4I_{11/2}$ state) or at 980 nm (excitation to the Yb^{3+} $^2F_{5/2}$ state). Excitation light was focused on the sample in a ~100 μm spot; the maximum power density was ~40 kW/cm^2. Luminescence was also excited at ~355 and ~520 nm (excitation to the $^2G_{9/2}$ and $^2H_{11/2}$ states of Er^{3+}, respectively) and a ns optical parametric oscillator (OPO) Lotis TII LT-2214 was used. Luminescence spectra were measured with a lock-in amplifier, a monochromator MDR-23 (SBW ~0.1 nm) as well as sensitive Hamamatsu S5345 and C5460-01 photodetectors. The spectral sensitivity of the set-up was accurately determined with a halogen lamp with calibrated spectral power density. The monochomator itself was calibrated with Pb and Xe lamps.

For the studies of luminescence decay, OPO with the pulse duration of ~20 ns was tuned to 355 or 960 nm. Luminescence was collected by a wide-aperture lens and re-imaged to the input slit of a monochromator MDR-12 (SBW~1 nm); then it was detected with fast Hamamatsu S5345 or C5460 photodetectors (response time, < 100 ns) and a 500 MHz Textronix TDS-3052B digital oscilloscope.

The CIE chromaticity coordinates of phosphors were calculated by using the photo luminescence data. All spectroscopic studies were performed at room temperature.

3. Results and discussion

Some as-grown crystals are shown in Fig. 1 and, as one can see, crystals demonstrate good optical quality. The XRD patterns of K_2YF_5, K_2ErF_5 and K_2YbF_5 are shown in Fig. 2 and they confirm that synthesized crystals have the orthorhombic lattice with similar unit cell dimensions, $a=10.820$ Å, $b=6.613$ Å, $c=7.249$ Å (for K_2YF_5), $a=10.813$ Å, $b=6.609$ Å, $c=7.245$ Å (for K_2ErF_5) and $a=10.765$ Å, $b=6.514$ Å, $c=7.203$ Å (for K_2YbF_5), see ICDD PDF Card-01-072-2387 [14,29]. Similar XRD patterns have been obtained for K_2YF_5 and K_2YbF_5 containing different Er^{3+} concentrations by confirming that all the compounds also crystallize into the pure orthorhombic phases, and Erbium doping does not lead to the formation of another crystal phase.

By using a 1 mm-thin plate made of the as-grown crystal, an absorption spectrum has been measured for 10 at% Er^{3+}:K_2YF_5 and it is shown in Fig. 3. Similar absorption characteristics are observed for Er^{3+}:K_2YbF_5 crystal which agrees with very similar

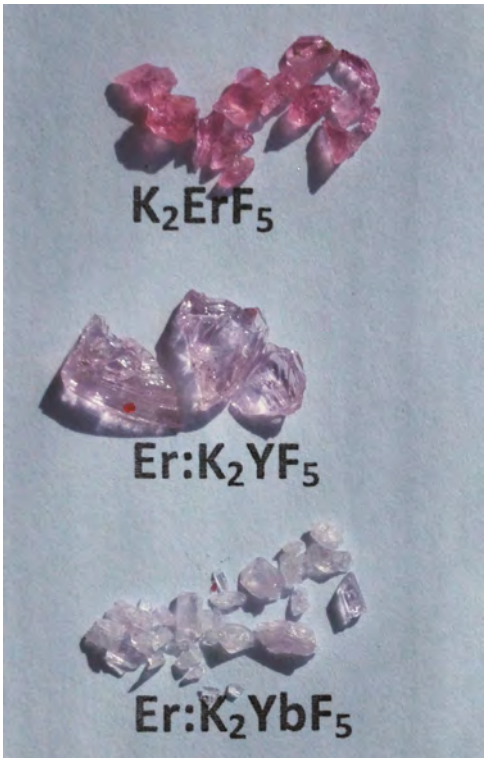

Fig. 1. Images of the studied Er-doped K_2YF_5 and K_2YbF_5 crystals.

structure of K_2YF_5 and K_2YbF_5 compounds [14]. Relatively high absorption oscillator strengths of f–f Er^{3+} transitions in the K_2YF_5 and K_2YbF_5 crystals are expected due to their anisotropic orthorhombic lattice and the distorted YF_7/YbF_7 coordination polyhedron [29]. The peak absorption coefficient α corresponding to the $^4I_{15/2}\rightarrow{}^4I_{11/2}$ transition is $\sim$1.0 cm^{-1} for 10 at% Er^{3+}:K_2YF_5 at $\sim$967 nm. Accordingly, the estimated peak absorption cross-section $\sigma_{abs}=\alpha/N_{Er}$ is $\sim 1.2\times10^{-21}$ cm^2 whereas the concentration of Er^{3+} ions in K_2YF_5, $N_{Er}=7.9\times10^{20}$ at/cm^3, has been calculated by taking into account that the unit cell volumes for K_2YF_5 and K_2ErF_5 are 518.7 and 517.7 $Å^3$, respectively, and the number of formula units is 4 as well as crystal densities ρ are 3.37 and 4.39 g/cm^3, respectively [14].

UCL spectra of the studied samples under the excitation at 960 nm to the Er^{3+} $^4I_{11/2}$ state are shown in Fig. 4. To assist with their interpretation, the schemes of energy levels for Er^{3+} and Yb^{3+} ions and relevant processes in the Er^{3+}–Yb^{3+} couple are shown in Fig. 5. For 10 at% Er^{3+}:K_2YF_5, the green emission band spanning from 510 to 580 nm and related to the transitions from the closely located and thermalized states $^2H_{11/2}$ and $^4S_{3/2}$ to the ground state $^4I_{15/2}$ dominates in the spectrum whereas the red emission in the range 640–700 nm related to the transition $^4F_{9/2}\rightarrow{}^4I_{15/2}$ is relatively weak. The ratio for integrated intensities of these bands (R/G ratio) is 1.28. These features determine the yellowish-green color of UCL from 10 at% Er^{3+}:K_2YF_5 in accordance with the CIE 1931 color space and, in particular, with the color coordinates $x=0.299$ and $y=0.695$ as well as high color purity, $p>99\%$, caused by the dominant wavelength at 549 nm.

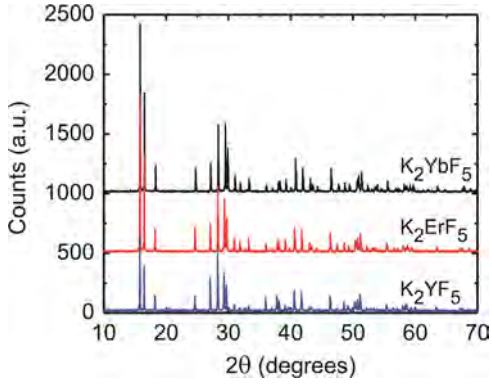

Fig. 2. X-ray diffraction patterns of K_2YF_5, K_2ErF_5 and K_2YbF_5.

For a stoichiometric K_2ErF_5 crystal, a significant redistribution of intensities between the green and red emission bands is observed in comparison with 10 at% Er^{3+}:K_2YF_5 and R/G ratio reaches 5.87. In addition, deep-red emission related to the transition $^4I_{9/2}\rightarrow{}^4I_{15/2}$ at $\sim$800 nm is enhanced. As a result, the color of UCL from K_2ErF_5 is yellow with $x=0.491$; $y=0.449$ and the 98% color purity, which is caused by the dominant wavelength of luminescence at 577 nm. It should be also noted that although the

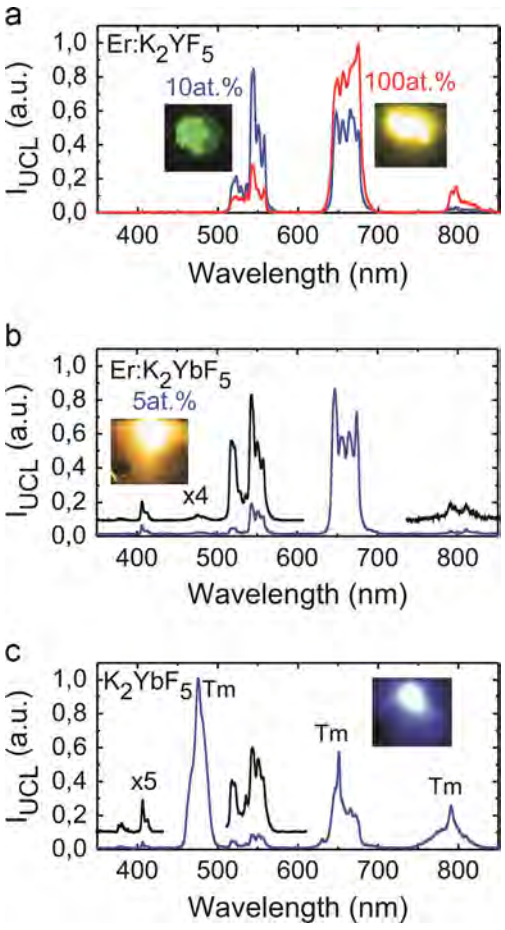

Fig. 4. Up-conversion luminescence (UCL) spectra of 10 at% Er^{3+}:K_2YF_5, K_2ErF_5 (a), 5 at% Er^{3+}:K_2YbF_5 (b) and K_2YbF_5 (c) crystals at RT; $\lambda_{exc}=960$ nm (a), 980 nm (b,c).

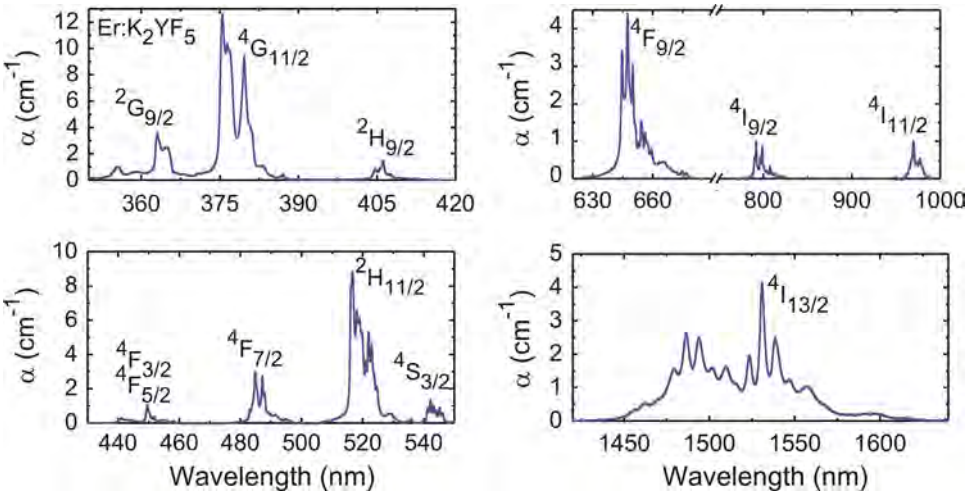

Fig. 3. Absorption spectra of the 10 at% Er^{3+}:K_2YF_5 crystal (background losses are subtracted) at RT.

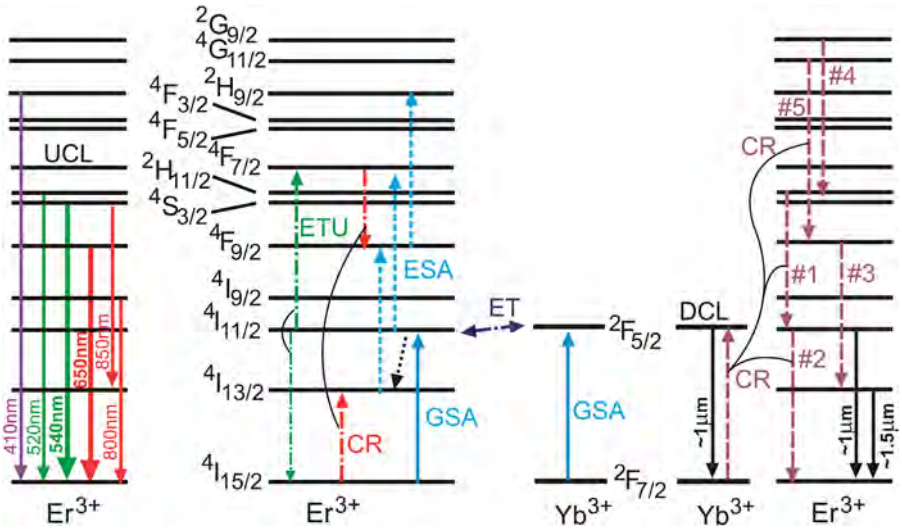

Fig. 5. The scheme of energy levels of Er^{3+} and Yb^{3+} ions showing the mechanisms of UCL: GSA and ESA – ground and excited-state absorption, CR – cross-relaxation, ET – energy transfer, ETU – energy transfer up-conversion, UCL – up-conversion luminescence, DCL – down-conversion luminescence.

Table 1
CIE 1931 color coordinates *x*, *y*, dominant wavelength λ_d and color purity *p* for luminescence from Er^{3+} doped fluoride crystals.

Crystal	*x*	*y*	λ_d (nm)	*p* (%)	Color
Exc. 960 nm					
10 at% Er^{3+}:K_2YF_5	0.299	0.695	549	99	Yellowish-green
K_2ErF_5	0.491	0.449	577	98	Yellow
5 at% Er^{3+}:K_2YbF_5	0.449	0.465	581	91	Yellow
Exc. 355 nm					
10 at% Er^{3+}:K_2YF_5	0.341	0.620	556	91	Yellowish-green
K_2ErF_5	0.348	0.557	558	74	Yellow-green
1 at% Er^{3+}:K_2YbF_5	0.498	0.293	–	–	Pink
5 at% Er^{3+}:K_2YbF_5	0.521	0.381	594	72	Orange

Er^{3+} concentration is relatively low, red emission is also dominant in the spectrum of 5 at% Er^{3+}:K_2YbF_5 with R/G=5.95 under excitation at 980 nm to the Yb^{3+} $^2F_{5/2}$ state and, as a result, the color of UCL from this crystal composition is also yellow with x=0.449; y=0.465. In the blue region there is a weak emission band which is due to the transition from the higher-lying excited state $^2H_{9/2}$ to the ground-state. Color characteristics for UCL from the studied crystals are summarized in Table 1.

In addition, UCL from an undoped K_2YbF_5 crystal has been studied under the excitation at 980 nm to the $^2F_{5/2}$ state of Yb^{3+}. The emission bands observed in Fig. 4(c) are due to ET from Yb^{3+} to impurity Er^{3+} and Tm^{3+} ions and UCL from Tm^{3+} is more intense. The bands centered at ~476, 650 and 790 nm are related to the transitions $^1G_4 \rightarrow {}^3H_6$, $^1G_4 \rightarrow {}^3F_4$ and $^3H_4 \rightarrow {}^3H_6$ for Tm^{3+}, respectively, whereas the green Er^{3+} emissions from the $^2H_{11/2}$ and $^4S_{3/2}$ states to the ground state $^4I_{15/2}$ are detected. The red Er^{3+} emission from the $^4F_{9/2}$ state at ~650 nm can overlap with the red Tm^{3+} one, so it is not discovered. Weak blue emissions from the $^4G_{11/2}$ and $^2H_{9/2}$ levels of the Er^{3+} ions are also detected at ~380 and 405 nm. Accordingly, UCL from the K_2YbF_5 crystal is blue–violet. It should be noted that cooperative emission from Yb^{3+}–Yb^{3+} ion pairs [30] is not detected for this K_2YbF_5 crystal at least for the excitation power density of ~50 kW/cm^2. This indicates relatively weak clustering of Yb^{3+} ions [31] or the cooperative emission of this type is overlapped by strong Tm^{3+} emission at ~476 nm.

In Fig. 6(a), log–log plots for the UCL intensity (I_{UCL}) versus the excitation power *P* are shown for a K_2ErF_5 crystal. For up-conversion process, I_{UCL} is proportional to the *n*th power of *P*, i.e. $I_{UCL} \sim P^n$ where *n* is the number of pump photons absorbed per up-converted photon emitted [32]. A plot of log I_{UCL} versus log *P* yields a straight line with slope *n*. For green emissions that occur from the $^2H_{11/2}$ and $^4S_{3/2}$ states, the slope of this dependence n=2.1 (521 nm and 543 nm), which means that two pump photons are required to populate the above mentioned states [33]. A pump wavelength of ~960 nm corresponds to ground-state absorption (GSA) due to the $^4I_{15/2} \rightarrow {}^4I_{11/2}$ transition. Further excitation can be due to excited state absorption (ESA) on the $^4I_{11/2} \rightarrow {}^4F_{7/2}$ transition or energy-transfer up-conversion (ETU) for adjacent Er^{3+} ions, $^4I_{11/2} + {}^4I_{11/2} \rightarrow {}^4I_{15/2} + {}^4F_{7/2}$. Taking into account fast non-radiative relaxation from the $^4F_{7/2}$ state, both $^2H_{11/2}$ and $^4S_{3/2}$ states are normally populated within a process that requires 2 pump photons, which is in agreement with Fig. 4(a). For red emission at 674 nm, n=2.0, too, by taking into account that the population of the $^4F_{9/2}$ state responsible for this emission occurs in three steps. These processes are GSA followed by non-radiative relaxation to the intermediate $^4I_{13/2}$ level and intense ESA thought the channel $^4I_{13/2} \rightarrow {}^4F_{9/2}$. It should be noted that although GSA for Er^{3+} doped crystals is weak (see Fig. 3), there is a mechanism that allows enhancing the excitation efficiency, namely cross-relaxation (CR), $^4I_{15/2} + {}^4F_{7/2} \rightarrow {}^4I_{13/2} + {}^4F_{9/2}$.

For crystals containing Er^{3+}–Yb^{3+} couples, excitation of Er^{3+} ions to the $^4I_{11/2}$ state can additionally occur via the energy transfer (ET) between the $^2F_{5/2}$ (Yb^{3+}) and $^4I_{11/2}$ (Er^{3+}) states that are nearly resonant in energy, Fig. 6(b). In this case normally 2 pump photons are also required for the population of the $^2H_{11/2}$ and $^4S_{3/2}$ states responsible for green UCL and the $^4F_{9/2}$ state responsible for red UCL. Indeed, in Fig. 6(b) slopes of the log–log plots for green UCL from the 5 at% Er^{3+}:K_2YbF_5 crystal are ~2. For the deep-red emission at ~790 nm due to the transition $^4I_{9/2} \rightarrow {}^4I_{15/2}$ the slope is ~1.9. The population of the $^4I_{9/2}$ state is realized through the population of the higher-lying $^4F_{9/2}$ state with subsequent non-radiative relaxation from $^4F_{9/2}$ to $^4I_{9/2}$ and, thus, this emission is also a consequence of a two-photon process. On the other hand, for blue UCL at ~410 nm that occurs from the $^2H_{9/2}$ state, the measured slope has amounted to 2.8, which means that 3 pump photons are required for populating this level. Indeed, there is the third intense ESA channel, $^4F_{9/2} \rightarrow {}^2H_{9/2}$, in order to realize this three-photon excitation process.

The near-IR emission spectrum for a stoichiometric K_2ErF_5 crystal is shown in Fig. 7. The observed emissions at ~1.5 and

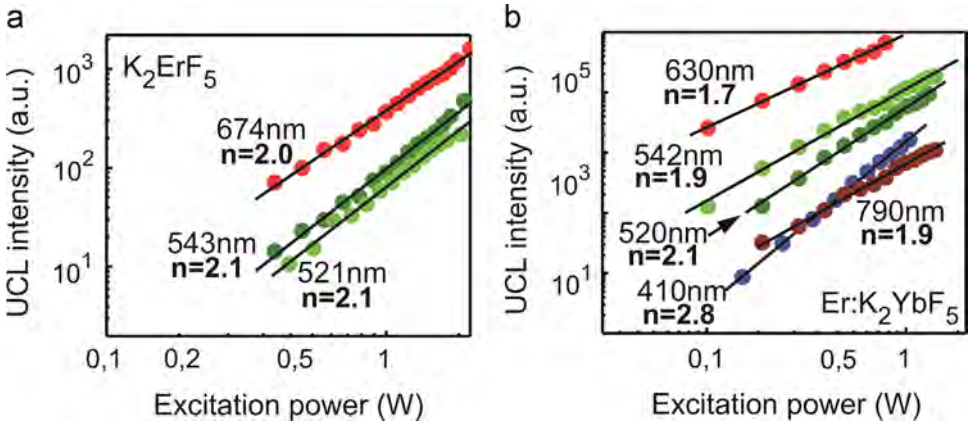

Fig. 6. Dependences of the UCL intensity on the excitation power for K_2ErF_5 (a) and 5 at% Er^{3+}:K_2YbF_5 (b) crystals at RT; λ_{exc}=960 nm (a) and 980 nm (b); *n* is the number of pump photons absorbed per up-converted photon emitted [32]. (For interpretation of the references to color in this figure, the reader is referred to the web version of this article.)

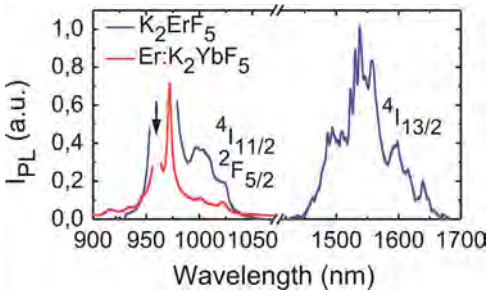

Fig. 7. Near-IR luminescence spectra of the K_2ErF_5 and 5 at% $Er^{3+}K_2YbF_5$ (b) crystals at RT; λ_{exc}=960 nm.

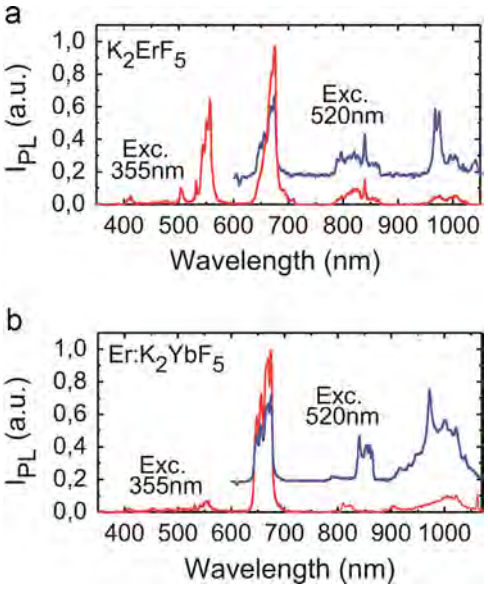

Fig. 8. Luminescence of K_2ErF_5 (a) and 5 at% Er^{3+}:K_2YbF_5 (b) crystals at RT after excitation into the $^2G_{9/2}$ state at 355 nm and into the $^2H_{11/2}$ state at 520 nm.

1 μm are due to the transitions from the $^4I_{13/2}$ and $^4I_{11/2}$ multiplets to the ground-state, respectively. For a 5 at% Er^{3+}:K_2YbF_5 crystal, the latter band is overlapped with a wide emission Yb^{3+} band ($^2F_{5/2}\rightarrow{}^2F_{7/2}$) spanning from 900 to 1050 nm.

Under excitation into the $^2G_{9/2}$ or the $^2H_{11/2}$ states at 355 nm or 520 nm, respectively, all the crystals singly doped with Er^{3+} ions demonstrate emission spectra (Fig. 8) similar to those obtained under near-IR excitation (Figs. 4 and 7). The corresponding color coordinates can be found in Table 1. However, for Er^{3+}:K_2YbF_5 crystals the spectra are different from those of Er^{3+} doped K_2YF_5 crystals. First, they differ from those obtained under near-IR excitation. As a result, pink (x=0.498, y=0.293) and orange (x=0.521, y=0.381) emissions are observed for 1 at% and 5 at% Er^{3+} doped K_2YbF_5, respectively (λ_{exc}=355 nm). This is due to a strong increase of the R/G ratio that reaches above 10. In addition, in the luminescence spectra of Er^{3+}:K_2YbF_5, a broad emission band spanning from 900 to 1050 nm is detected. This effect is particularly evident under 520 nm excitation when the intensity of the near-IR emission is enhanced with respect to the red one. This broad near-IR band can be attributed to the emission on the $^2F_{5/2}\rightarrow{}^2F_{7/2}$ transition of Yb^{3+} ions excited through the down-conversion (DC) process [8,12].

DC for the Er^{3+}–Yb^{3+} couple includes several CR processes, which can be also phonon-assisted [8,11,12], resulting in de-excitation of the Er^{3+} ion and simultaneous excitation of adjacent Yb^{3+} ions emitting at ~1 μm, Fig. 8(b). For 520 nm excitation, there are two possible DC schemes. The first scheme is based on two de-excitation steps, namely CR #1 [$^4S_{3/2}(Er^{3+})+{}^2F_{7/2}(Yb^{3+})\rightarrow{}^4I_{11/2}(Er^{3+})+{}^2F_{5/2}(Yb^{3+})$] and CR #2 [$^4I_{11/2}(Er^{3+})+{}^2F_{7/2}(Yb^{3+})\rightarrow{}^4I_{15/2}(Er^{3+})+{}^2F_{5/2}(Yb^{3+})$]. Alternatively to CR #2, Er^{3+} ions can emit near infrared radiation at about 1 μm due to the $^4I_{11/2}\rightarrow{}^4I_{15/2}$ transition. This scheme corresponds to the emission of 2 photons at ~1 μm. However, this DC process has a relatively low probability as several phonons are required to compensate the energy mismatch for CR #1. The second scheme is CR #3 [$^4F_{9/2}(Er^{3+})+{}^2F_{7/2}(Yb^{3+})\rightarrow{}^4I_{13/2}(Er^{3+})+{}^2F_{5/2}(Yb^{3+})$] that provides 1 photon at ~1 μm and subsequent Er^{3+} emission at ~1.5 μm due to the $^4I_{13/2}\rightarrow{}^4I_{15/2}$ transition. Thus, in both cases two near-IR photons are emitted.

For 355 nm excitation into the $^2G_{9/2}$ state, there are few possible schemes involving CR processes that can provide ~1 μm emission, for instance, phonon-assisted processes CR #4 [$^2G_{9/2}(Er^{3+})+{}^2F_{7/2}(Yb^{3+})\rightarrow{}^2H_{11/2}(Er^{3+})+{}^2F_{5/2}(Yb^{3+})$] or CR #5 [$^4G_{11/2}(Er^{3+})+{}^2F_{7/2}(Yb^{3+})\rightarrow{}^4F_{9/2}(Er^{3+})+{}^2F_{5/2}(Yb^{3+})$]. Both processes terminate on the Er^{3+} states responsible for visible emission, namely green and red emissions at 520 and 650 nm. Thus, under 355 nm excitation DC seems to lead to the generation of one near-IR and one visible photon in both versions. Alternatively, but with a much lower probability, the second de-excitation step can be provided by processes CR #1–CR #3. This difference is clear from Fig. 8(b), by taking into account that under 520 nm excitation the relative intensity of near-IR emission at ~1 μm is much higher as compared with that under 355 nm excitation as well as that red emission from the $^4F_{9/2}$ state is dominating in the latter case. For

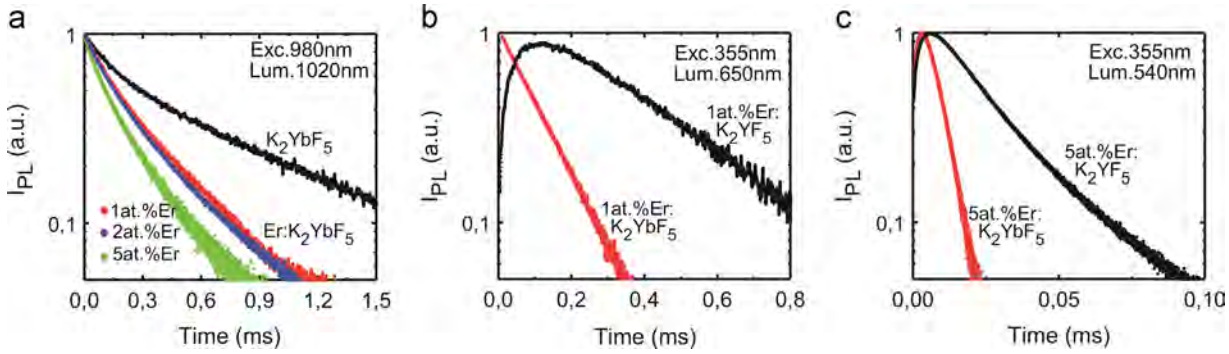

Fig. 9. Shortening of the lifetime of the $^2F_{5/2}$ state of Yb^{3+} ions for Er^{3+}:K_2YbF_5 crystals as compared with the K_2YbF_5 one (a); shortening of the lifetimes of the $^4F_{9/2}$ (b) and $^4S_{3/2}$ (c) states of Er^{3+} ions in K_2YbF_5 crystals as compared with Er^{3+}:K_2YF_5 ones. The measurements were performed at RT.

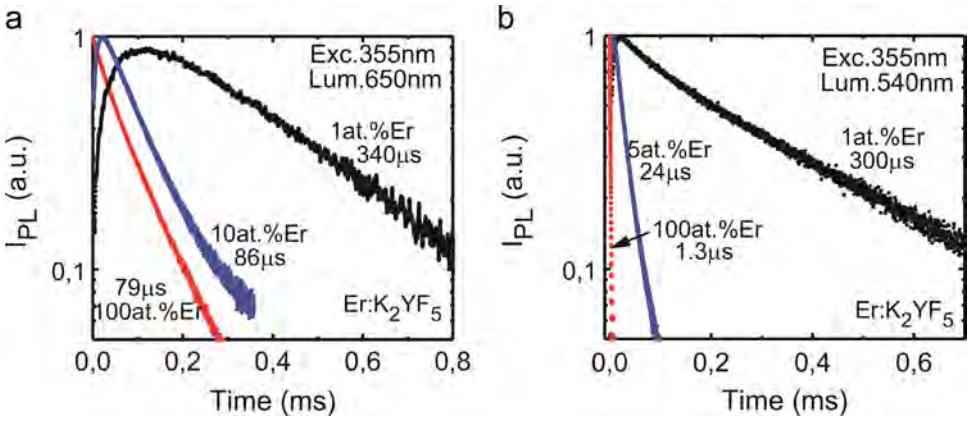

Fig. 10. Decay curves for visible Er^{3+} emissions from the $^4F_{9/2}$ (a) and $^4S_{3/2}$ (b) states versus the Er^{3+} concentration in K_2YF_5 crystals; λ_{exc}=355 nm. The measurements were performed at RT.

illustration, the schemes of the above mentioned UCL and DCL processes are shown in Fig. 5.

To determine the efficiency of ET for the $^2F_{5/2}$ (Yb^{3+})→$^4I_{11/2}$ (Er^{3+}) process in the Er^{3+}:K_2YbF_5 crystals, the lifetimes of the Yb^{3+} $^2F_{5/2}$ excited state in an undoped K_2YbF_5 crystal and K_2YbF_5 crystals doped with 1, 2 and 5 at% Er^{3+} have been measured and the decay curves for the Yb^{3+} emission at 1020 nm are shown in Fig. 9(a). The lifetimes have been determined on the 1/*e* level by using the excitation wavelength of 980 nm. For donor Yb^{3+} ions in undoped K_2YbF_5, the lifetime τ_D(Yb) is 580 μs whereas for K_2YbF_5 containing acceptor Er^{3+} ions, the measured lifetimes τ_{D-A}(Yb) are reduced to 274, 245 and 192 μs for 1, 2 and 5 at% Er^{3+}, respectively. Thus, the efficiency of ET, $\eta_{ET}=1-\tau_{D-A}/\tau_D$, equals 53%, 58% and 67% and the probabilities of energy transfer are then $p_{ET}=(1/\tau_{D-A})-(1/\tau_D)$=1920, 2360 and 3480 s^{-1} for 1, 2 and 5 at% Er^{3+}, respectively. The increase of η_{ET} with the increase of the Er^{3+} content means that it can be even higher under a higher Er/Yb ratio.

To estimate the efficiency of the energy transfer η_{ET} from Er^{3+} to Yb^{3+} ions resulting in the down-conversion luminescence, the decay times for red and green emissions at ~550 and 650 nm for Er^{3+} doped K_2YF_5 and Er^{3+} doped K_2YbF_5 crystals have been measured under the 355 nm wavelength excitation into the $^2G_{9/2}$ state, Fig. 9(b) and (c). For Er^{3+}:K_2YF_5 crystals, there is a clear build-up at the beginning of the decay curves for red emission due to multiphonon relaxation from the $^4G_{9/2}$ state to the $^4F_{9/2}$ one. The build-up nearly disappears for the K_2YbF_5 crystals doped with Er^{3+} ions, because in this case the $^4F_{9/2}$ level is efficiently populated through cross relaxation with neighboring Yb^{3+} ion (process CR #5). This observation provides an additional evidence for down-conversion through the quantum cutting mechanism in Er^{3+} doped K_2YbF_5 crystals. The decay time for the $^4F_{9/2}$ emission is 340 μs for the 1 at% Er^{3+}:K_2YF_5 crystal and it is shortened to 114 μs for the 1 at% Er^{3+}:K_2YbF_5 one, resulting in the 66% efficiency of the Er^{3+}→Yb^{3+} ET from the $^4F_{9/2}$ state. Similarly for green emission from the $^4S_{3/2}$ state, in this case cross-relaxation scheme CR #4 is also involved in the decay process. Accordingly, it leads to shortening of the rise time for green emission, Fig. 9(c). The decay time for the $^4S_{3/2}$ emission is also shortened from 21 μs for the 5 at% Er^{3+}:K_2YF_5 crystal to 6.4 μs for the 5 at% Er^{3+}:K_2YbF_5 one. The estimated efficiency of the Er^{3+}→Yb^{3+} ET from the $^4S_{3/2}$ state is ~69%.

The determined efficiency of ET from Er^{3+} to Yb^{3+} for 5 at% Er^{3+} doped K_2YbF_5 is higher than η_{ET}=28% discovered for 1 at% Er^{3+}, 30 at% Yb^{3+} doped $NaYF_4$ [12]. This may be attributed to the higher doping levels of both Er^{3+} and Yb^{3+} which can be reached without the considerable concentration quenching due to the crystal chemical peculiarities of the K_2YF_5 structure. In this context, it should be noted that the achieved efficiency of ET in Er^{3+}:K_2YbF_5 is approaching the results obtained for the Tb^{3+}–Yb^{3+}, the Tm^{3+}–Yb^{3+} and the Pr^{3+}–Yb^{3+} couples, η_{ET} ~80% to 90%, in which down-conversion is based on a cooperative energy transfer from the appropriate rare-earth ion to a couple of adjacent Yb^{3+} ions [34–36].

The dependences of the lifetimes on the Er^{3+} concentration for both the $^4F_{9/2}$ and the $^4S_{3/2}$ states in the Er^{3+}:K_2YF_5 crystals are shown in Fig. 10. For 1 at% Er^{3+}:K_2YF_5, the decay time of the red emission is 340 μs and it is shortened to 86 μs for 10 at% Er:K_2YF_5. However, the further increase of the Er^{3+} concentration does not lead to significant reduction of the $^4F_{9/2}$ lifetime and for stoichiometric K_2ErF_5 it is 79 μs. In contrast, for the green emission from the $^4S_{3/2}$ state, the lifetime is 300 μs for 1 at% Er^{3+} doping and it is as short as 1.3 μs for stoichiometric K_2ErF_5. This explains the observed redistribution of intensity between the green and red

Table 2
Measured lifetimes of the excited-states for K_2ErF_5 crystals at RT.

Ref.	$^4I_{13/2}$ (ms)	$^4I_{11/2}$ (μs)	$^4I_{9/2}$ (μs)	$^4F_{9/2}$ (μs)	$^2S_{3/2}$ (μs)
This paper	3.1	61	149	79	1.3
[23]	1.07	200	–	–	2

emission bands in the UCL spectrum depending on an Er^{3+} concentration in K_2YF_5 crystals, Fig. 4(a).

The measured lifetimes of the excited states from $^4I_{13/2}$ to $^4S_{3/2}$ for a K_2ErF_5 crystal are collected in Table 2 and they are compared with data published before [27]. The contrast in the values measured in this work and presented in Ref. [27] may be due to the different purity degree of the starting Er_2O_3 oxides used for synthesis and the other impurity rare earth types in the oxides. Such impurities can considerably change efficiency of ET between the rare earth ions [37]. For K_2ErF_5 synthesized within this research the lifetime of the $^4I_{13/2}$ state is ~3.1 ms. Such a long lifetime for the 100 at% Er-doped crystal is a feature of fluoride materials with a low phonon frequencies. For $^4I_{11/2}$ state, the lifetime is relatively short, 61 μs. This peculiarity indicates the suitability of the K_2ErF_5 crystal for laser operation.

4. Conclusions

To conclude, we report on growth and detailed spectroscopic study of Er^{3+}-doped K_2YF_5 and K_2YbF_5 fluorides as well as stoichiometric composition K_2ErF_5. Their absorption, visible and near-IR luminescence have been studied. For a 5 at% Er^{3+}:K_2YbF_5 crystal, the efficiency of ET from Yb^{3+} to Er^{3+} is as high as 67%. Under near-IR excitation by an InGaAs laser diode at 980 nm, this crystal provides intense yellow UCL. Under excitation in the UV/visible range at 355 and 532 nm, a clear evidence of the down-conversion process is observed and the efficiency of ET from Er^{3+} to Yb^{3+} reaches 69%. In other words, K_2YbF_5 doped with Er^{3+} is a very attractive combination for developing luminescent up- and down-converters for enhancing the performance of solar cells. For Er^{3+}:K_2YF_5 crystals when the doping level is changed from 10 to 100 at%, the color tunability for the UCL from yellow–green to yellow is detected. To explain it, lifetimes of the excited states for $^4I_{13/2}$ and $^4S_{3/2}$ levels have been measured. In particular, for K_2ErF_5 the lifetime of the $^4I_{13/2}$ state is ~3.1 ms and the lifetime of the $^4I_{11/2}$ state is relatively short, 61 μs. This also indicates the potential of highly-doped Er:K_2YF_5 crystals for laser applications.

Acknowledgments

This research was partially supported by the Russian Foundation for Basic Research (Research Project no. 15-03-02507a); Fundación CajaCanarias (Grant No. AY06) within the project MAGEC (Materials for Advanced Generation of Energy at Canary Islands); and the Spanish Ministry of Economy and Competitiveness (Project ENE2013-47826-C4-4-R).

References

[1] F. Auzel, D. Pecile, D. Morin, J. Electrochem. Soc. 122 (1975) 101.
[2] G. Liu, Chem. Soc. Rev. 44 (2015) 1635.
[3] K.W. Krämer, D. Biner, G. Frei, H.U. Güdel, M.P. Hehlen, S.R. Lüthi, Chem. Mater. 16 (2004) 1244.
[4] G. Yi, H. Lu, S. Zhao, Y. Ge, W. Yang, D. Chen, L.-H. Guo, Nano Lett. 4 (2004) 2191.
[5] W. Zheng, P. Huang, D. Tu, E. Ma, H. Zhu, X. Chen, Chem. Soc. Rev. 44 (2015) 1379.
[6] A. Shalav, B.S. Richards, T. Trupke, K.W. Krämer, H.U. Güdel, Appl. Phys. Lett. 86 (2005) 013505.
[7] R. Brede, E. Heumann, J. Koetke, T. Danger, G. Huber, B. Chai, Appl. Phys. Lett. 63 (1993) 2030.
[8] V.D. Rodriguez, V.K. Tikhomirov, J. Mendez-Ramos, A.C. Yanes, V. V. Moshchalkov, Sol. Energy Mater. Sol. Cells 94 (2010) 1612.
[9] W. Zheng, H. Zhu, R. Li, D. Tu, Y. Liu, W. Luo, X. Chen, Phys. Chem. Chem. Phys. 14 (2012) 6974.
[10] J.T. van Wijngaarden, S. Scheidelaar, T.J.H. Vlugt, M.F. Reid, A. Meijerink, Phys. Rev. B 81 (2010) 155112-1.
[11] J.J. Eilers, D. Biner, J.T. van Wijngaarden, K. Krämer, H.-U. Güdel, A. Meijerink, Appl. Phys. Lett. 96 (2010) 151106.
[12] L. Aarts, B.M. van der Ende, A. Meijerink, J. Appl. Phys. 106 (2009) 023522.
[13] N. Martin, R. Mahiou, P. Boutinaud, J.C. Cousseins, J. Alloy. Cmpd. 323–324 (2001) 303.
[14] N.M. Khaidukov, P.P. Fedorov, L.N. Dem'yanets, I.P. Zibrov, V.A. Malyusov, Russ. J. Inorg. Chem. 35 (1990) 383.
[15] D. Wang, Y. Min, S. Xia, V.N. Makhov, N.M. Khaidukov, J.C. Krupa, J. Alloy. Compd. 368 (2004) 337.
[16] D. Wang, Y. Min, S. Xia, V.N. Makhov, N.M. Khaidukov, J.C. Krupa, J. Alloy. Compd. 361 (2003) 294.
[17] M. Yin, Y. Li, N. Dong, V.N. Makhov, N.M. Khaidukov, J.C. Krupa, J. Alloy. Cmpd. 353 (2003) 95.
[18] Z. Kollia, E. Sarantopoulou, A.C. Cefalas, A.K. Naumov, V.V. Semashko, R. Y. Abdulsabirov, S.L. Korableva, Opt. Commun. 149 (1998) 386.
[19] M.A. Dubinskii, N.M. Khaidukov, I.G. Garipov, L.N. Dem'yanets, A.K. Naumov, V. V. Semashko, V.A. Malyusov, J. Mod. Opt. 37 (1990) 1355.
[20] P. Boutinaud, R. Mahiou, J.C. Cousseins, J. Lumin. 72–74 (1997) 318.
[21] J. Marcazzó, N.M. Khaidukov, E. Caselli, C. Dangelo, M. Santiago, Phys. Status Solidi A 206 (2009) 2593.
[22] J.C. Min Yin, E. Krupa, Antic-Fidancev, V.N. Makhov, N.M. Khaidukov, J. Lumin. 101 (2003) 79.
[23] V.N. Makhov, N.M. Khaidukov, D. Lo, M. Kirm, G. Zimmerer, J. Lumin. 102–103 (2003) 638.
[24] J. Marcazzy, P. Molina, F. Ortega, M. Santiago, F. Spano, N. Khaidukov, E. Caselli, Radiat. Meas. 43 (2008) 208.
[25] D. Wang, Y. Guo, Q. Wang, Z. Chang, J. Liu, J. Luo, J. Alloy. Compd. 474 (2009) 23.
[26] Y. Li, M. Yin, N. Dong, V.N. Makhov, N.M. Khaidukov, J.C. Krupa, J. Phys. Chem. Solids 65 (2004) 1059.
[27] R.E. Peale, H. Weidner, F.G. Anderson, N.M. Khaidukov, Adv. Solid State Lasers 10 (1997) 462.
[28] J. Mendez-Ramos, P. Acosta-Mora, J.C. Ruiz-Morales, N.M. Khaidukov, J. Alloy. Compd. 575 (2013) 263.
[29] F. Loncke, D. Zverev, H. Vrielinck, N.M. Khaidukov, P. Matthys, F. Callens, Phys. Rev. B 75 (2007) 144427-1.
[30] F. Auzel, P. Goldner, Opt. Mater. 16 (2001) 93.
[31] P.A. Loiko, G.E. Rachkovskaya, G.B. Zakharevich, A.A. Kornienko, E.B. Dunina, A. S. Yasukevich, K.V. Yumashev, J. Non-Cryst. Solids 392–393 (2014) 39.
[32] X.M. Li, H. Guo, Y.L. Wei, Y.R. Guo, H. Lu, H.M. Noh, J.H. Jeong, J. Lumin. 152 (2014) 168.
[33] M. Pollnau, D.R. Gamelin, S.R. Luthi, H.U. Gudel, Phys. Rev. B 61 (2000) 3337.
[34] J.L. Yuan, X.Y. Zeng, J.T. Zhao, Z.J. Zhang, H.H. Chen, X.X. Yang, J. Phys. D 41 (2008) 105406.
[35] G. Lakshminarayana, H. Yang, S. Ye, Y. Liu, J. Qiu, J. Mater. Res. 23 (2008) 3090.
[36] G. Lakshminarayana, H. Yang, S. Ye, Y. Liu, J. Qiu, J. Phys. D 41 (2008) 175111.
[37] J.P. Jouart, M. Bouffard, T. Duvaut, N.M. Khaidukov, Chem. Phys. Lett. 366 (2002) 62.